Paleoredox and lithogeochemical indicators of the environment of formation and genesis of the Monster River hyper-enriched black shale showing, Yukon

M.G. Gadd[1*], J.M. Peter[1], T.A. Fraser[2], and D. Layton-Matthews[3]

Gadd, M.G., Peter, J.M., Fraser, T.A., and Layton-Matthews, D., 2022. Paleoredox and lithogeochemical indicators of the environment of formation and genesis of the Monster River hyper-enriched black shale showing, Yukon; in *Targeted Geoscience Initiative 5: volcanic- and sediment-hosted massive-sulfide deposit genesis and exploration methods, (ed.) J.M. Peter and M.G. Gadd; Geological Survey of Canada, Bulletin 617, p. 113–127. https://doi.org/10.4095/328004*

Abstract: Northern Yukon hosts occurrences of Middle Devonian hyper-enriched black shale (HEBS) Ni-Mo-Zn–platinum-group element-Au-Re mineralization, including the Monster River showing in the Ogilvie Mountains. This mineralization has been documented predominantly in the Paleozoic Richardson trough; however, the Monster River showing is atypical, occurring within the Blackstone trough, more than 200 km to the west on the southern margin of the Yukon block. The ambient paleoredox conditions of the marine water column and sediments may be primary controlling factors in HEBS formation. We use major and trace element lithogeochemistry to better understand ambient paleoenvironmental redox conditions through the application of robust redox proxies to HEBS mineralization and host rocks. Uniformly negative Ce anomalies (0.6–0.9) indicate that the water column was predominantly suboxic throughout the deposition interval, even during HEBS mineralization. Although there is a strong terrigenous influence on the rare earth element–yttrium (REE-Y) abundances of the sedimentary rocks, superchondritic Y/Ho ratios (>27) indicate that seawater contributed REE-Y to the host rocks and HEBS. High (>10) authigenic Mo/U ratios indicate that a Fe-Mn particulate shuttle operated in the water column; this is corroborated by negative Ce anomalies and high Y/Ho ratios. The data indicate that metalliferous sedimentary rocks formed by hydrogenous metal enrichment (e.g. Ni, Mo, Pt) caused by ferromanganese oxyhydroxide particulate shuttling as chemical sediments; moreover, the REE- and Mo-based paleoenvironmental indicators suggest a complexly redox-stratified depositional environment with an abundant supply of metals, metalloids, and sulfur.

Résumé : Le nord du Yukon renferme des indices d'une minéralisation à Ni-Mo-Zn–éléments du groupe du platine-Au-Re dans des shales noirs surenrichis du Dévonien moyen, dont l'indice de Monster River dans les monts Ogilvie. Cette minéralisation a surtout été documentée dans la cuvette de Richardson du Paléozoïque; cependant, l'indice de Monster River est atypique, puisqu'il se situe dans la cuvette de Blackstone, plus de 200 km à l'ouest de la bordure sud du bloc du Yukon. Les paléoconditions ambiantes d'oxydoréduction dans la colonne d'eau marine et les sédiments pourraient constituer les principaux facteurs déterminants de la formation des shales noirs surenrichis. Nous avons utilisé la lithogéochimie des éléments majeurs et en traces pour mieux comprendre les conditions paléoenvironnementales d'oxydoréduction ambiantes en ayant recours à de solides indicateurs indirects des conditions d'oxydoréduction au sein de la minéralisation de shales noirs surenrichis et des roches hôtes. Des anomalies uniformément négatives en Ce (0,6-0,9) indiquent que les conditions dans la colonne d'eau étaient surtout suboxiques tout au long de l'intervalle de dépôt, même au cours de l'épisode de minéralisation de shales noirs surenrichis. Bien qu'il y ait une forte influence terrigène dans l'abondance des éléments de terres rares-yttrium (ÉTR-Y) dans les roches sédimentaires, des rapports Y/Ho superchondritiques (>27) montrent que l'eau de mer a fourni les ÉTR-Y aux roches hôtes et aux shales noirs surenrichis. Des rapports Mo/U authigènes élevés (>10) indiquent que des particules d'oxyhydroxyde de Fe-Mn se déplaçaient dans la colonne d'eau, ce qui est corroboré par les anomalies négatives en Ce et les rapports Y/Ho élevés. Les données montrent que des roches sédimentaires métallifères ont été formées par un enrichissement en métaux hydrogéniques (p. ex. Ni, Mo et Pt) provoqué par le déplacement de particules de Fe-Mn en tant que sédiments chimiques. De plus, les indicateurs paléoenvironnementaux fondés sur les ÉTR et Mo laissent entrevoir un milieu sédimentaire complexe présentant une stratification des conditions d'oxydoréduction dans lequel existait une abondante source de métaux, de métalloïdes et de soufre.

[1]Geological Survey of Canada, 601 Booth Street, Ottawa, Ontario K1A 0E8
[2]Yukon Geological Survey, P.O. Box 2703 (K-14), Whitehorse, Yukon Territory, Y1A 2C6
[3]Queen's University, Department of Geological Sciences and Geological Engineering, Bruce Wing/Miller Hall, 36 Union Street, Kingston, Ontario K7L 3N6
*Corresponding author: M.G. Gadd (email: michael.gadd@nrcan-rncan.gc.ca)

INTRODUCTION

Hyper-enriched black shales (HEBS; also referred to as polymetallic shales) are regionally extensive in northern Yukon and are documented at several localities covering thousands of square kilometres (Fig. 1). At the Nick Ni-Mo-Zn–platinum-group element (PGE)-Au-Re prospect, the first documented site of this style of mineralization in Yukon, the nickeliferous horizon is thin (3–10 cm) and discontinuously crops out in several stream cuts (Carne, 1989). Although this is the most studied HEBS property in Yukon (Hulbert et al., 1992; Horan et al., 1994; Orberger et al., 2003a, b, 2005; Pagès et al., 2018; Pasava et al., 2018; Gadd et al., 2020), there are other HEBS showings in northern Yukon (Fig. 1). These other localities have been the focus of recent investigations, including HEBS at Peel River (Gadd et al., 2017, 2019b, 2020; Gadd and Peter, 2018; Crawford et al., 2019) and Moss (Gadd et al., 2019a).

A lack of understanding of how these deposits formed hinders exploration, and there currently is no consensus on the HEBS genetic model. Seafloor hydrothermal venting (Hulbert et al., 1992; Steiner et al., 2001) and hydrogenous (seawater) scavenging (Lehmann et al., 2007, 2016; Xu et al., 2011, 2013) are the two models that have received the most attention. In either model, ambient paleoenvironmental reduction-oxidation (redox) conditions must have played a significant role in the formation and preservation of the HEBS because the enrichment of metals occurred on the seafloor or within the shallow subsurface; however, determination of ancient depositional conditions is commonly impeded by incomplete sedimentary records and/or post-depositional modifications to primary signatures.

To overcome this, we used bulk and trace-element geochemical compositions and proxies of organic carbon-rich shales. The proxies are based on the behaviour of redox-sensitive elements in modern marine environments and are able to resolve oxic (>2 mL O_2/L H_2O), suboxic (0.2–2 mL O_2/L H_2O), anoxic (0 mL O_2/L H_2O), and euxinic (>0 mL H_2S/L H_2O) environments (Tribovillard et al., 2006). Particularly robust paleoredox proxies include rare-earth element (REE)–Y (e.g. Ce; Wallace et al., 2017) and Mo and U (Algeo and Tribovillard, 2009) because they withstand moderate to intense diagenesis and low-grade metamorphism.

We focus here on the lesser known Monster River HEBS locality (lat. 64°50′5.14″N, long. 140°32′23.50″W) in the Ogilvie Mountains. At the Monster River showing, the 2 to 5 cm thick HEBS layer has the same characteristic elemental enrichment as other HEBS localities across Yukon. Previous exploration efforts at Monster River did not identify the HEBS horizon (Dumala, 2007); however, our fieldwork in 2018 located the HEBS layer at the same stratigraphic level as in other localities. In this paper, we present a detailed lithogeochemical and paleoredox evaluation of the HEBS mineralization and immediate host rocks at Monster River. This research provides insight into some of the physical and chemical factors that control HEBS formation, including basinal redox stratification, availability of metals, very low sedimentation rate, and high biological productivity.

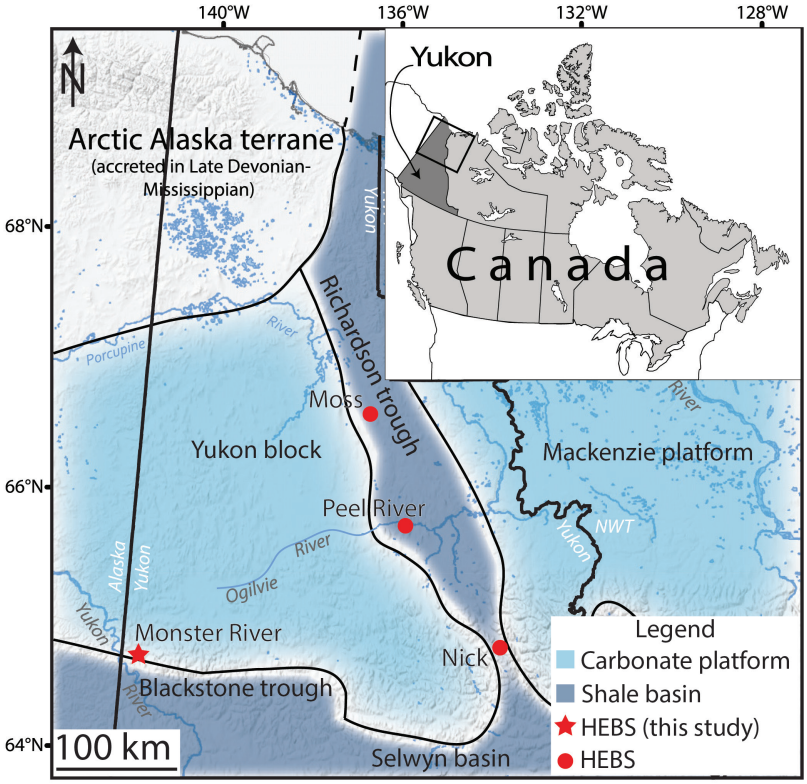

Figure 1. Map of Middle Devonian paleogeographic elements (light blue, carbonate platforms; dark blue, basins) on the Laurentian continental margin with hyper-enriched black shale (HEBS) at Monster River (red star) and other HEBS localities (red circles; *modified from* Fraser and Hutchison (2017) *after* Morrow and Geldsetzer (1988) and Morrow (1999)). Note that the location of Blackstone trough is approximate.

The conclusions of this study provide broader regional insight into the setting and genetic process(es) of HEBS mineralization in the northern Canadian Cordillera.

LOCATION, REGIONAL STRATIGRAPHY, AND AGE OF HEBS

Paleozoic sediments in northern Yukon were deposited as a series of platforms and basins on the margin of Laurentia (ancestral North America). Most documented HEBS occurrences in northern Yukon occur within the Richardson trough, an intracratonic basin that separated the Mackenzie platform and the Yukon block carbonate platform during the early Paleozoic (Fig. 1; Lenz, 1972; Pugh, 1983; Cecile et al., 1997; Norris, 1997; Morrow, 1999). The Monster River showing, however, is located farther west (present day) of Richardson trough, on the southern margin of the Yukon block within Paleozoic strata of the Blackstone trough (Fig. 1). In both basins, late Cambrian to Middle Devonian strata consist of fine-grained, variably calcareous siliciclastic rocks of the Road River Group (Fig. 2a; e.g. Jackson and Lenz, 1962; Norris, 1985, 1997; Morrow, 1999). Overlying the Road River Group sedimentary rocks is siliceous-cherty shale of the Late Devonian Canol Formation (Richardson trough, Yukon block; e.g. Norris, 1985, 1997; Morrow, 1999; Fraser and Hutchison, 2017) and the lower part of the Earn Group (Selwyn basin; e.g. Portrait Lake Formation of Gordey and Anderson (1993)). The nature of the contact between the Road River Group and the overlying Canol Formation has been variably interpreted as conformable, disconformable, and unconformable (e.g. Pugh, 1983;

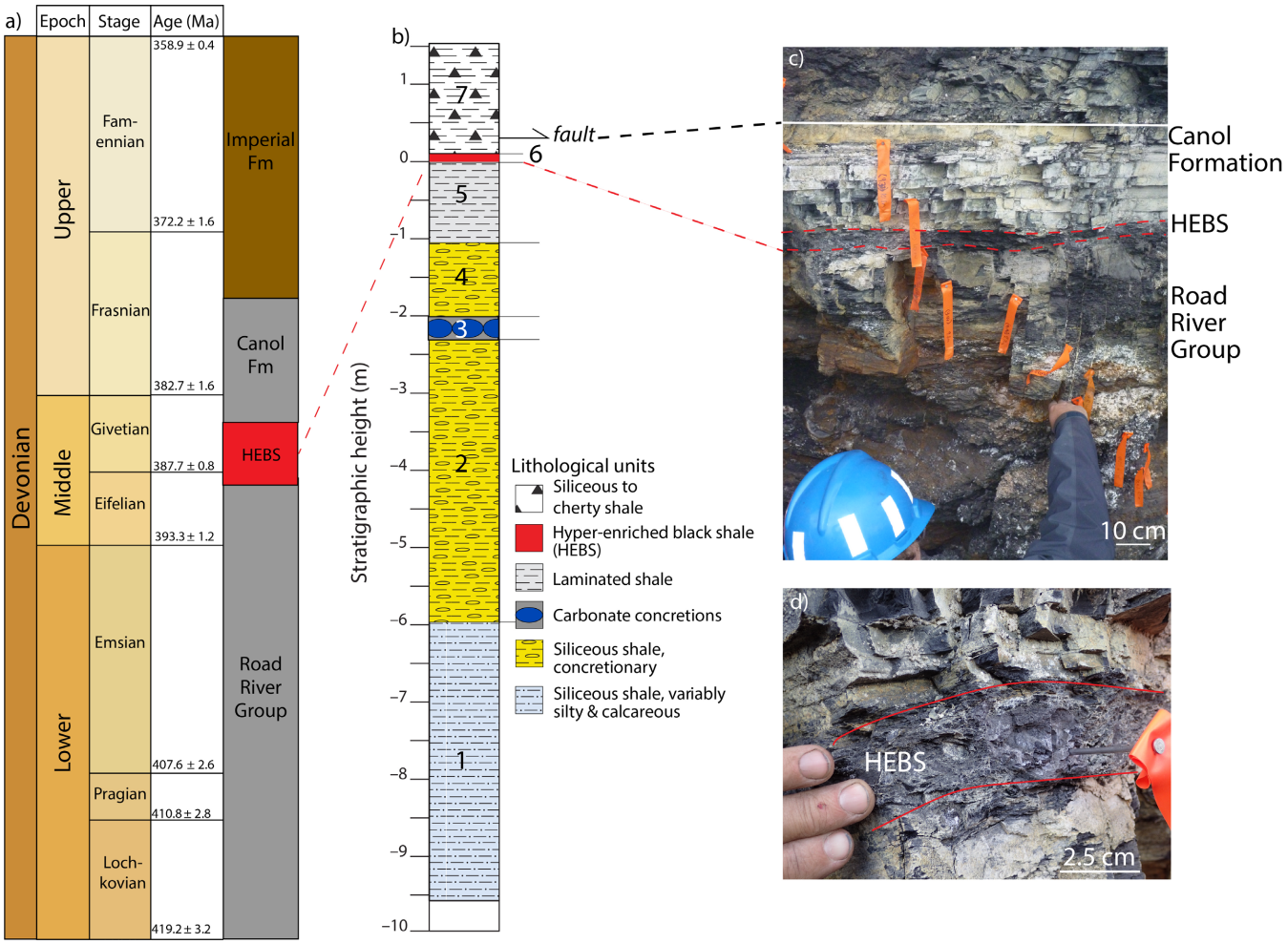

Figure 2. Stratigraphy at the Monster River showing: **a)** stratigraphic section of Devonian basinal sediments in the study areausing the timescale of Becker et al. (2012) with stratigraphic age of units *modified from* Fraser and Hutchison (2017) to include updated hyper-enriched black shale (HEBS) dates *after* S.A. Gouwy, unpub. rept. (2019); **b)** graphical log of lithostratigraphy at the Monster River HEBS showing; **c)** photograph of the upper portion of the stratigraphic succession at Monster River showing the HEBS layer outlined in red and the fault line in white. The orange tape marks sample locations at 10 cm spacing. Photograph by J.M. Peter. NRCan Photo 2020-123; **d)** close-up photograph of the HEBS unit. Note the sharp contact with the overlying shale and chert of the Canol Formation. Photograph courtesy of T.A. Fraser, Yukon Geological Survey

Morrow, 1999; Fraser and Hutchison, 2017). At this contact, a discontinuous, thin (1–10 cm thick) Ni-Mo-Zn-PGE–rich HEBS layer (previously called the 'NiMo' or 'Nick' horizon) has been identified at several localities throughout northern Yukon. At all localities in Yukon, HEBS mineralization is enriched in a broad suite of elements relative to the enclosing sedimentary rocks, including Ni, Mo, Zn, PGE, Au, and Re (Hulbert et al., 1992; Gadd and Peter, 2018; Gadd, Peter, and Layton-Matthews, this volume).

Conodonts recovered from HEBS samples at the Monster River locality indicate a Middle Devonian age of deposition (S.A. Gouwy, unpub. rept., 2019). The age range of conodonts is identical to the HEBS at Peel River (Gadd et al., 2020) and is slightly younger than conodonts recovered from 1.5 m below the HEBS at the Nick prospect (Gadd et al., 2020). Horan et al. (1994) conducted Re-Os isotope analyses of the HEBS layer and host black shales at the Nick prospect. They concluded that metal enrichment occurred during or shortly after deposition of the host rocks, and that the age of mineralization is between 380 and 367 Ma. New, refined isochron ages (Gadd et al., 2020) from Peel River and Nick reveal HEBS ages of 387.5 ± 4.4 and 390.7 ± 5.1 Ma, respectively, indicating coeval formation of HEBS across the region.

METHODS

Sampling and lithogeochemistry

Shale and semi-massive sulfide samples were collected from outcrop at the Monster River showing. The samples were collected at 10 cm intervals from the Canol Formation through to 2.5 m below the HEBS layer, and at 50 cm stratigraphic intervals below that. Despite our best efforts to collect fresh (i.e. non-weathered) samples, surficial exposure has resulted in weak to intense chemical weathering. This is most pronounced within the HEBS, where primary minerals are preserved but secondary minerals are also present. The most conspicuous secondary mineral is nickelhexahydrite (identified by X-ray diffraction), a hydrated NiS mineral that is a product of oxidation of nickel sulfide minerals (i.e. millerite; Jambor et al., 2000).

Bulk samples were homogenized over a sampled stratigraphic interval (e.g. 0.1 to 0.5 m) of stratigraphy for lithogeochemical analyses and submitted to ALS Global in North Vancouver, British Columbia for analysis. Samples were crushed and splits were ground to <63 µm in a ceramic mill. Quartz sand was milled between each sample to clean the mill and prevent cross-contamination. Major and refractory trace elements were measured in 5 g splits using a lithium metaborate/tetraborate fusion followed by inductively coupled plasma–mass spectrometry (ICP-MS). Trace elements were measured in 0.5 g splits using a four-acid (HCl-HNO_3-$HClO_4$-HF) digestion followed by ICP-MS analysis. To measure Ru, Rh, Pd, Os, Ir, Pt, and Au content, 10 to 25 g splits were preconcentrated in NiS beads produced by fire assay prior to ICP-MS analysis. The abundance of C (i.e. C_{org} and CO_2) and S was determined using infrared mass spectrometry.

Data treatment

Measured REE-Y abundances were normalized against post-Archean Australian shale (PAAS; McLennan, 1989). The PAAS-normalized values are marked with subscript 'N'. Anomalies, denoted by '*' are quantified ratios determined using the geometric means of the neighbouring elements following the convention of McLennan (1989): $Ce/Ce^* = Ce_N/(La_N \times Pr_N)^{0.5}$, $Eu/Eu^* = Eu_N/(Sm_N \times Gd_N)^{0.5}$. Elemental enrichment factors (EF) are expressed as X_{EF}, where X is an element of interest (Algeo and Tribovillard, 2009), and are calculated using the expression $(X/Al_2O_3)_{sample}/(X/Al_2O_3)_{PAAS}$.

RESULTS

Lithostratigraphy

The measured section at the Monster River HEBS showing is composed of seven lithological units (Fig. 2b), described here in stratigraphic order from bottom to top. Unit 1 (3.6 m thick) is dark grey to black, siliceous, finely laminated shale that is variably silty. The rocks occur as stacked sets of upward-fining laminated sequences (30–50 cm thick) with scoured basal contacts. The unit contains up to 5% oblong pyrite concretions (generally ≤8 cm long x 1 cm high, although may be up to 30 cm long x 5 cm high) along discrete bedding planes, graptolites, and accessory gypsum crystals on bedding surfaces. Unit 2 (3.7 m thick) is black, siliceous shale with up to 15 volume % barite concretions (mainly 3 cm long x 2 cm high) with minor larger carbonate concretions (≤75 cm long x 40 cm high). The shale is laminated and is locally silty, graptolitic, and contains gypsum. The lower contact of this unit is gradational, and the upper contact is sharp with unit 3. Unit 3 (0.20 m thick) is a distinctive, resistant layer of large, semi-continuous, elongated carbonate concretions, which pinch and swell, are internally laminated, and form sharp contacts with overlying and underlying units. Unit 4 (1.0 m thick) is characterized by black, siliceous, well-indurated, finely laminated shale with ≤5% small ovoid (≤4 cm wide x 2 cm high) pyrite and barite concretions. Unit 5 is similar to unit 4 but has fewer concretions and is distinctly well laminated (Fig. 2c, d). Unit 6 (2–5 cm thick) is the HEBS layer, comprising stratabound, stratiform, semi-massive Ni-Mo-Zn-Fe–sulfide mineralization and interstratified shale (Fig. 2c, d). This unit is black on fresh surfaces, and weathers dark grey, mint green, and orange. Laminae in the unit are wavy parallel, and upper and lower contacts are sharp with surrounding sedimentary rocks. Unit 7 is composed of siliceous to cherty, laminated

to thinly bedded black shale in sharp contact with the underlying HEBS mineralization. The top of the stratigraphic section is truncated by a (?)thrust fault about 20 cm above the HEBS contact with the Canol Formation.

Lithogeochemistry

Elemental abundance ranges and geochemical proxies are presented in Table 1 for: a) unmineralized host black shales of the Road River Group (footwall), b) HEBS mineralization, and c) Canol Formation carbonaceous siliceous shales and carbonaceous cherty shales (hanging wall).

Road River Group sedimentary rocks, when compared to PAAS (McLennan, 1989), can be characterized by major-element composition: shale-like SiO_2 contents (Fig. 3a), low to high carbonate contents (Fig. 3b), low $Fe_2O_{3(tot)}$ contents (Fig. 3c), moderate to shale-like terrigenous input, (contents TIP = $Al_2O_3 + TiO_2 + K_2O + Na_2O$; Fig. 3d; Fraser and Hutchison, 2017), high total S (Fig. 3e), moderate to high total organic carbon (TOC) contents (Fig. 3f), and high to very high (4–85 x PAAS) Mo contents (Fig. 3g). The Road River Group rocks also possess weakly to moderately negative Ce/Ce* anomalies (<1; Fig. 3h), crustal (also chondritic; ca. 27; Taylor and McLennan, 1995) to superchondritic (>27) Y/Ho ratios (Fig. 3i), and low to moderate (<10) Mo_{EF}/U_{EF} ratios (Fig. 3j).

The HEBS layer, when compared to PAAS (McLennan, 1989), is characterized by low SiO_2 contents (Fig. 3a), high carbonate contents (Fig. 3b), extremely high Fe_2O_3(tot) contents (Fig. 3c), low TIP (Fig. 3d) contents, extremely high total S (Fig. 3e), high TOC contents (Fig. 3f), and extremely high (650–764 x PAAS) Mo contents (Fig. 3g). The HEBS layer also possesses weak to moderate negative Ce/Ce* anomalies (Fig. 3h), superchondritic Y/Ho ratios (Fig. 3i), and extremely high (>>10) Mo_{EF}/U_{EF} ratios (Fig. 3j).

The Canol Formation, when compared to PAAS (McLennan, 1989), is characterized by very high SiO_2 contents (Fig. 3a), very low carbonate contents (Fig. 3b), low Fe_2O_3(tot) contents (Fig. 3c), low TIP (Fig. 3d) contents, high total S (Fig. 3e), high TOC contents (Fig. 3f), and very high (30 x PAAS) Mo contents (Fig. 3g). The Canol Formation also possesses moderate negative Ce/Ce* anomalies (Fig. 3h), superchondritic Y/Ho ratios (Fig. 3i), and high (>10) Mo_{EF}/U_{EF} ratios (Fig. 3j).

DISCUSSION

Rare-earth element–yttrium geochemistry

The REE-Y abundances provide important information about the conditions under which sedimentary rocks were deposited (e.g. Wright et al., 1987; McLennan, 1989; Peter et al., 2003; Lode et al., 2015). At Monster River, REE-Y abundances correlate with phosphate abundance (Fig. 4a), which is itself probably related to apatite abundance. Apatite is a common accessory mineral in HEBS (Gadd and Peter, 2018) and if formed authigenically, may sequester REE-Y from the ambient paleoenvironment (e.g. Gadd et al., 2016). The TIP fraction likely contributes some REE-Y, based on its prevalence at the Moss HEBS showing (Gadd et al., 2019a), but this is minor compared to apatite. Regardless of the host phase, PAAS-normalized REE-Y profiles reveal important information about the conditions under which sediments were deposited and the evolution of the sedimentary porewaters. Representative lithostratigraphic samples show that the REE-Y profiles are mostly flat with minor deviations (Fig. 4b). Flat topology of the PAAS-normalized REE-Y profiles indicates a normal, shale-like pattern (i.e. no fractionation from average shale), whereas deviations from flat profiles (e.g. convex upward) may indicate depositional or post-depositional modifications to REE-Y (Reynard et al., 1999).

Systematic changes to REE behaviour in sediment porewaters are commonly attributed to anoxic diagenesis (e.g. Himmler et al., 2010). This occurs because middle REE (MREE; Sm, Eu, Gd) are mobilized from metastable phases within the sediment pile (e.g. ferromanganese particles and labile organic matter; Hu et al., 2014) into authigenic precipitates (e.g. carbonate minerals; Himmler et al., 2010). Representative REE-Y profiles of the different lithostratigraphic units show minor convex upward 'humps' (Fig. 4b), suggesting remobilization occurred at a localized scale within the shallow subsurface. This is interpreted to reflect the complex diagenesis of the rocks that host HEBS. Although this remobilization may have affected Eu anomalies, it is unlikely to have significantly affected Ce anomalies and Y/Ho ratios (*see* below).

Among the lanthanide series elements, only Ce and Eu deviate from the trivalent state. At Monster River, and within other HEBS in Yukon, Eu anomalies are weakly positive to nil (Table 1; Crawford et al., 2019; Gadd et al., 2019a; Gadd, Peter, and Layton-Matthews, this volume; Pagès et al., 2018). Cerium has two valences, Ce^{3+} and Ce^{4+}, and the relative abundances are principally controlled by redox; Ce fractionates relative to adjacent La and Pr based primarily on the ambient oxidation state (De Baar et al., 1988). Cerium (III) is the dominant ion in oxygenated marine environments; it is transformed to Ce^{4+} during oxidative scavenging by particle-reactive Fe-Mn–oxyhydroxides (Elderfield and Greaves, 1982). The magnitude of Ce depletion is controlled by water depth; surface waters in modern oxygenated marine environments typically do not to have Ce anomalies. Progressive scavenging of Ce at depth by Fe-Mn particles results in significant Ce depletion in marine waters (Nozaki, 1997; Alibo and Nozaki, 1999). Phases that precipitate or adsorb REE from Ce-depleted marine waters have negative Ce anomalies (defined by Ce/Ce* <1). Cerium in anoxic marine conditions is like other trivalent REEs with no anomalous fractionation (Ce/Ce* 1), due to ferromanganese particulate dissolution (German and

Table 1. Summary of lithogeochemical data for the Monster River locality.

Chemical symbol	Unit	LLOD	Analytical method	Road River Group		Hyper-enriched black shale		Canol Formation
			Range of abundances		Mean (n=38)	Range of abundances	Mean (n=4)	Range of abundances (n=2)
SiO_2	wt %	0.01	Fusion–ICP-ES	34.9–67.5	54.49	33.8–39.3	37.93	83.6–85
Al_2O_3	wt %	0.01	Fusion–ICP-ES	8–16.85	13.04	4.64–5.9	5.46	3.66–4.86
CaO	wt %	0.01	Fusion–ICP-ES	0.64–11.4	3	3.72–5.49	4.46	0.1–0.17
Fe_2O_3	wt %	0.01	Fusion–ICP-ES	2.73–7.57	4.85	14.1–15.9	14.78	0.88–1.42
MgO	wt %	0.01	Fusion–ICP-ES	0.83–7.27	2.15	0.3–0.36	0.34	0.26–0.36
Na_2O	wt %	0.01	Fusion–ICP-ES	0.47–0.71	0.6	0.16–0.2	0.18	0.13–0.16
K_2O	wt %	0.01	Fusion–ICP-ES	1.99–4.76	3.71	1.27–1.63	1.5	0.88–1.18
Cr_2O_3	wt %	0.001	Fusion–ICP-ES	0.012–0.022	0.02	0.013–0.016	0.02	0.01–0.015
TiO_2	wt %	0.01	Fusion–ICP-ES	0.49–1.77	1.16	0.24–0.5	0.33	0.18–0.25
MnO	wt %	0.01	Fusion–ICP-ES	0.01–0.07	0.03	0.01–0.01	0.01	LLOD
P_2O_5	wt %	0.01	Fusion–ICP-ES	0.16–1.51	0.48	2.61–3.98	3.16	0.07–0.08
SrO	wt %	0.01	Fusion–ICP-ES	0.01–0.1	0.02	0.02–0.03	0.03	0.01–0.01
BaO	wt %	0.01	Fusion–ICP-ES	0.23–21.9	2.21	0.34–0.42	0.38	0.31–0.82
H_2O	wt %	0.01	Leco	1.41–5.94	4.15	LLOD	LLOD	1.82–3.16
LOI	wt %	0.01	Leco	10.1–20.7	13.2	22–26.2	23.2	8.59–9.81
Total C	wt %	0.01	Leco	2.35–7.41	3.56	4.08–5.66	4.94	4.66–6.06
Total S	wt %	0.01	Leco	1.97–7.21	3.72	15.25–17.35	15.98	0.58–0.82
CO_2	wt %	0.2	Coulometer	0.2–15.5	2.8	LLOD	LLOD	LLOD
Corg	wt %	0.01	Leco	1.77–4.39	2.78	3.98–5.57	4.88	4.62–5.93
Ssulfide	wt %	0.01	Leco	1.6–5.28	2.73	11.7–14.55	13.41	0.24–0.26
Li	ppm	0.2	Four-acid	14–120.5	37.6	10.2–13.7	12.1	15.9–16.8
Sc	ppm	0.1	Four-acid	8.3–20.2	14.1	6.5–9.3	7.7	3.3–4.9
V	ppm	5	Fusion–ICP-MS	496–2310	1230	539–763	660	924–1410
Co	ppm	0.1	Four-acid	7.8–27.3	17.1	331–536	459.8	2.1–2.3
Ni	ppm	0.2	Four-acid	109.5–847	317.7	30300–53900	44000	297–391
Cu	ppm	0.2	Four-acid	40.8–151	63.1	359–449	418	38.3–52.7
Zn	ppm	2	Four-acid	243–3410	1460.3	1580–4780	2650	242–242
Ga	ppm	0.1	Fusion–ICP-MS	11.9–27.4	20	10.3–11.6	11	6.9–8.5
As	ppm	0.1	Aqua regia	15.6–109.5	39.1	2180–2730	2532.5	14–19.2
Se	ppm	0.2	Aqua regia	10.8–74.8	24.3	1900–3200	2700	36.4–40.8
Rb	ppm	0.2	Fusion–ICP-MS	66.5–147	112.7	35.3–44.3	41.5	36.2–49.6
Zr	ppm	2	Fusion–ICP-MS	100–337	233	63–81	75	58–70
Nb	ppm	0.2	Fusion–ICP-MS	11–61.7	38.4	7.9–20.7	11.8	4.6–6
Mo	ppm	0.05	Four-acid	7.99–85.1	21.66	650–764	704.75	29.8–29.9
Ag	ppm	0.01	Four-acid	0.81–3.75	1.98	5.25–6.29	5.845	1.24–1.98
Cd	ppm	0.02	Four-acid	2.13–57.9	24.55	20.6–34.1	25.95	3.69–4.52
In	ppm	0.005	Aqua regia	0.02–0.12	0.06	0.05–0.08	0.065	0.01–0.02
Sn	ppm	1	Fusion–ICP-MS	1–3	2	1–1	1	0–0
Sb	ppm	0.05	Aqua regia	10.9–23.8	16.52	146–202	186.13	7.43–9.41
Te	ppm	0.01	Aqua regia	0.08–0.18	0.11	19.05–46.2	36.36	0.13–0.21
Cs	ppm	0.01	Fusion–ICP-MS	3.28–8.72	5.94	1.8–2.17	2.02	2.49–3.21
La	ppm	0.5	Fusion–ICP-MS	22.2–101	50.3	89.9–107.5	103	12.6–16.1
Ce	ppm	0.5	Fusion–ICP-MS	39.8–172.5	82.2	120.5–135.5	124.9	17.3–22.2
Pr	ppm	0.03	Fusion–ICP-MS	4.98–25.7	11.83	23.1–25.9	23.88	2.59–3.72
Nd	ppm	0.1	Fusion–ICP-MS	18.2–109.5	46.5	92.7–102	95.3	10–14.4
Sm	ppm	0.03	Fusion–ICP-MS	2.95–22.2	9.12	16.45–18.75	17.525	1.55–1.79

Table 1. (cont.) Summary of lithogeochemical data for the Monster River locality.

Chemical symbol	Unit	LLOD	Analytical method	Road River Group		Hyper-enriched black shale		Canol Formation
			Range of abundances		Mean (n=38)	Range of abundances	Mean (n=4)	Range of abundances (n=2)
Eu	ppm	0.03	Fusion–ICP-MS	0.58–5.46	2.11	4.19–4.71	4.4675	0.27–0.27
Gd	ppm	0.05	Fusion–ICP-MS	2.38–22	8.94	19.45–20.9	20.1875	1.23–1.46
Tb	ppm	0.01	Fusion–ICP-MS	0.39–3.15	1.29	2.72–2.89	2.79	0.19–0.24
Dy	ppm	0.05	Fusion–ICP-MS	2.54–17.9	7.43	15.85–16.35	16.13	1.22–1.73
Y	ppm	0.5	Fusion–ICP-MS	18.2–119	47.3	138.5–154.5	147.3	9.7–14.8
Ho	ppm	0.01	Fusion–ICP-MS	0.51–3.22	1.43	3.19–3.31	3.26	0.3–0.41
Er	ppm	0.03	Fusion–ICP-MS	1.87–9.3	4.18	9.06–9.19	9.13	0.93–1.42
Tm	ppm	0.01	Fusion–ICP-MS	0.27–1.11	0.57	1.01–1.16	1.07	0.15–0.2
Yb	ppm	0.03	Fusion–ICP-MS	1.94–6.64	3.64	5.74–6.55	6.2	0.97–1.34
Lu	ppm	0.01	Fusion–ICP-MS	0.27–0.86	0.53	0.76–0.94	0.85	0.15–0.25
Hf	ppm	0.2	Fusion–ICP-MS	2.5–8.3	5.7	1.3–1.8	1.6	1.3–1.4
Ta	ppm	0.1	Fusion–ICP-MS	0.8–3.7	2.3	0.4–0.6	0.6	0.3–0.4
W	ppm	1	Fusion–ICP-MS	1–3	2	1–1	1	1–3
Re	ppm	0.001	Aqua regia	0.007–0.149	0.039	20.3–32.7	27.575	0.075–0.084
Hg	ppm	0.005	Aqua regia	0.113–0.379	0.212	3.35–4.95	4.298	0.129–0.18
Tl	ppm	0.02	Aqua regia	0.12–3.3	0.73	41.6–84.9	53.55	0.11–0.67
Pb	ppm	0.01	Aqua regia	11.7–22.3	18.34	62.6–76.7	66.98	3.7–5.5
Bi	ppm	0.5	Four-acid	0.1–0.37	0.2	1–1.66	1.4	0.08–0.09
Th	ppm	0.05	Fusion–ICP-MS	5.34–11.55	9.35	2.83–3.4	3.15	2.53–2.67
U	ppm	0.05	Fusion–ICP-MS	6.14–41.2	17.5	83.4–92	89.13	6.93–7.97
Pt	ppb	1	NiS bead; ICP-MS	<1–18	4	264–342	307	9–14
Pd	ppb	1	NiS bead; ICP-MS	<1–14	6	124–183	160	9–17
Au	ppb	2	NiS bead; ICP-MS	<2–149	23	42–54	50	LLOD
Rh	ppb	1	NiS bead; ICP-MS	LLOD	2	2–6	3.3	LLOD
Ir	ppb	2	NiS bead; ICP-MS	<1–1	1	2–4	3	<1–1
Os	ppb	5	NiS bead; ICP-MS	<2–4	2	44–96	7.5	3–7
Ru	ppb	2	NiS bead; ICP-MS	<2–12	6	<2–17	13	LLOD
Ce/Ce*	n/a	n/a	n/a	0.66–0.84	0.78	0.55–0.62	0.58	0.66–0.7
Pr/Pr*	n/a	n/a	n/a	1.04–1.18	1.09	1.23–1.25	1.25	1.12–1.18
Eu/Eu*	n/a	n/a	n/a	0.72–1.23	1.05	1.08–1.14	1.11	0.78–0.91
Y/Ho	n/a	n/a	n/a	27.16–42.6	32.5	43.42–46.96	45.15	32.33–36.1
$(La/Sm)_N$	n/a	n/a	n/a	0.56–1.25	0.83	0.72–0.95	0.86	1.18–1.31
$(La/Yb)_N$	n/a	n/a	n/a	0.77–1.26	1.02	1.1–1.38	1.23	0.89–0.96
$(Sm/Yb)_N$	n/a	n/a	n/a	0.77–1.93	1.26	1.28–1.66	1.45	0.68–0.81
Mo_{EF}	n/a	n/a	n/a	10–117	32.81	2174–2940	2465.85	116–153
U_{EF}	n/a	n/a	n/a	3–18	8.69	95–110	100.06	9–13
Mo_{EF}/U_{EF}	n/a	n/a	n/a	2–9	3.78	22–27	24.57	12–13

EF: enrichment factor; Four-acid: four-acid digestion using HCl, HNO_3, $HClO_4$, and HF; Fusion: lithium metaborate/tetraborate fusion; ICP-ES: inductively coupled plasma–emission spectrometry; ICP-MS: inductively coupled plasma–mass spectrometry; Leco: Combustion analysis; LLOD: lower limit of detection; LOI: loss-on-ignition; subscript N: post-Archaean Australian shale (PAAS)–normalized; *denotes quantified ratios determined using the geometric means of the neighbouring elements following the convention of McLennan (1989)

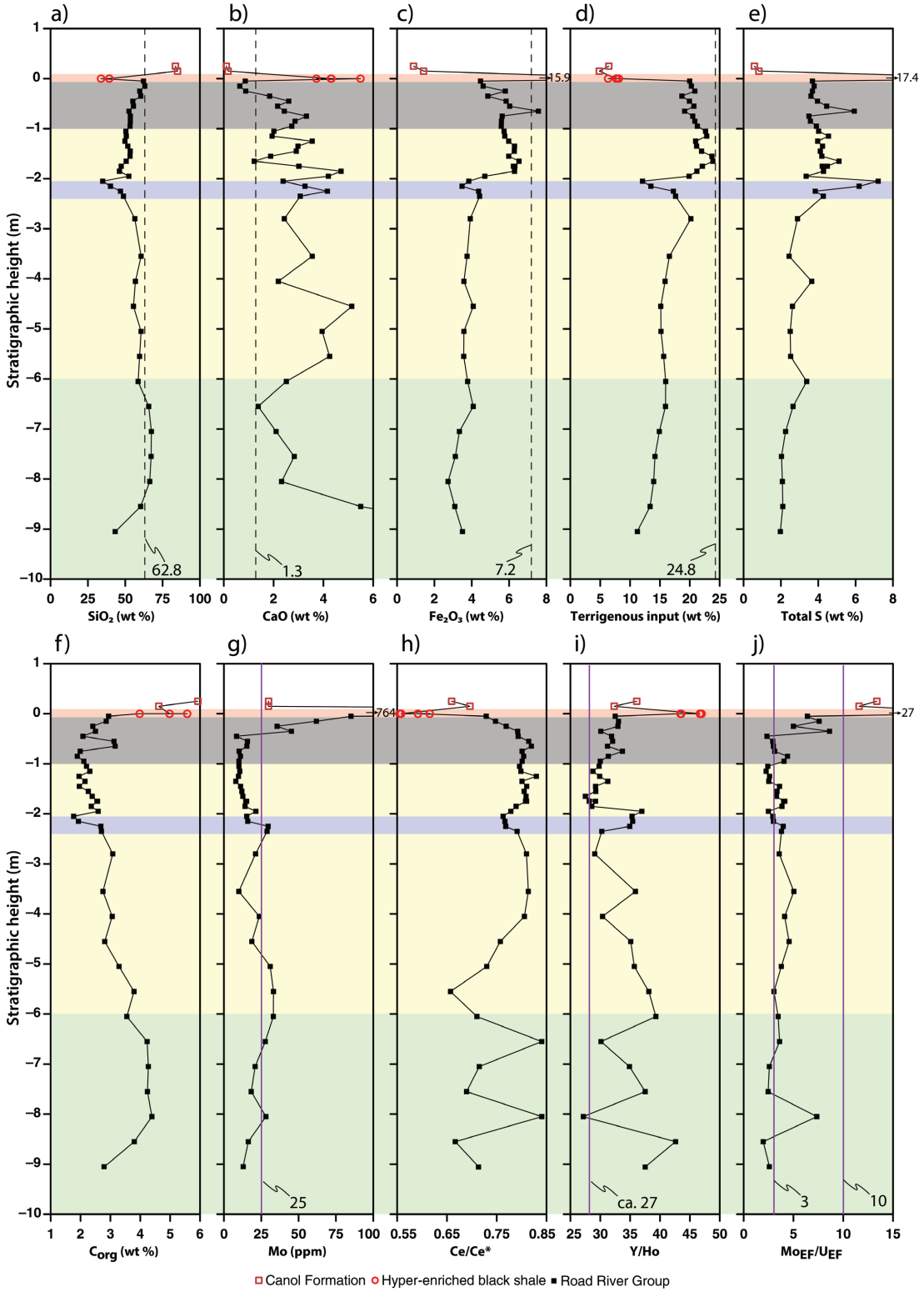

Figure 3. Lithostratigraphic profiles of selected elements, oxides, and element ratios for the Monster River hyper-enriched black shale (HEBS) at an outcrop in Ogilvie Mountains based on bulk rock analyses. The '0 m' stratigraphic marker defines the bottom of the HEBS mineralized zone, with strata above assigned to the Canol Formation and below to the Road River Group: **a)** SiO_2; **b)** CaO; **c)** total Fe_2O_3; **d)** terrigenous input (Al_2O_3 + TiO_2 + K_2O + Na_2O); **e)** total S; **f)** total organic carbon; **g)** Mo; **h)** Ce/Ce* (post-Archaean Australian shale (PAAS)–normalized); **i)** Y/Ho; **j)** Mo_{EF}/U_{EF}. Note: the shaded colours correspond to lithostratigraphic units in Figure 2; dashed vertical lines correspond to PAAS values and solid vertical purple lines correspond to proxy threshold values described in the text.

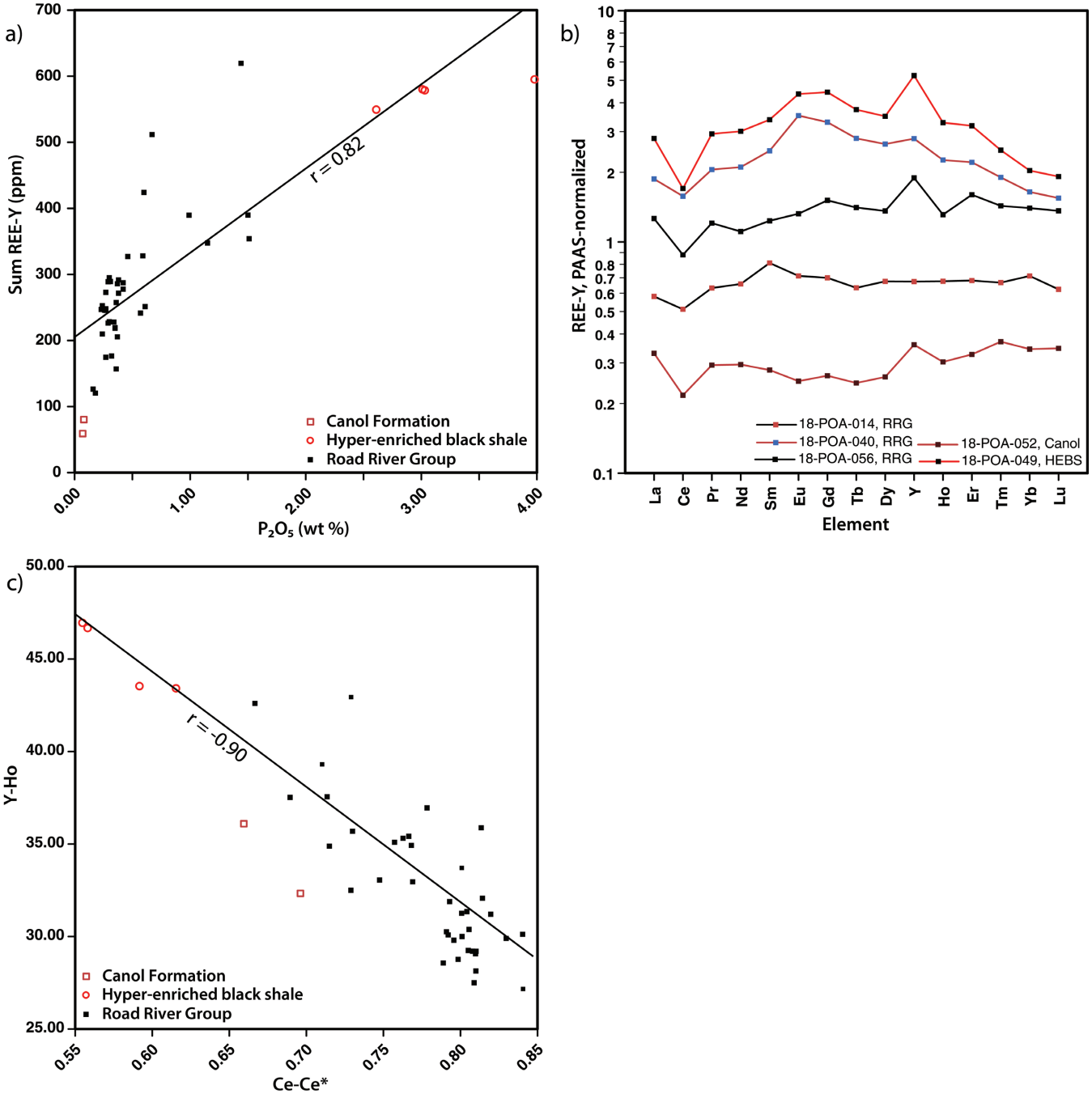

Figure 4. Rare-earth element (REE)–Y geochemistry from samples of the Canol Formation, hyper-enriched black shale (HEBS), and Road River Group (RRG) rocks at the Monster River showing: **a)** bivariate plot of ΣREE-Y versus P_2O_5 abundance; **b)** plot of representative post-Archaean Australian shale (PAAS)–normalized REE-Y abundances for different lithostratigraphic samples; **c)** bivariate plot of Y/Ho versus Ce/Ce*.

Elderfield, 1990). In ancient sedimentary rocks, Ce anomalies generally remain robust and are minimally affected by diagenesis, burial, metamorphism, and weathering (Slack et al., 2009, Lode et al., 2015).

The Monster River mineralization and host rock samples possess exclusively negative Ce/Ce* values, regardless of stratigraphic position (Fig. 3h, 4b–c). These anomalies are real and not imparted by anomalous La behaviour, based on comparisons with Pr/Pr* (not shown; Bau and Dulski, 1996). Cerium anomalies with values between 0.4 and 0.9 indicate deposition under suboxic bottomwater conditions (Tribovillard et al., 2006). The Ce/Ce* values show minor fluctuation within the lower 5 m of the Road River Group that stabilize at approximately 0.8 from 4.0 to 0.5 m below the HEBS (Fig. 3h). Above this point and through to the HEBS, Ce/Ce* values systematically decrease (Fig. 3h). This trend of decreasing Ce/Ce* values is also observed at the Moss showing (Gadd et al., 2019a). This suggests that the water column became more oxygenated, resulting in enhanced Fe oxyhydroxide scavenging (Bau, 1999) immediately preceding, and during, the HEBS formation. The presence of negative Ce anomalies in the sulfide mineralization is somewhat counterintuitive. Formation and preservation of semi-massive sulfide layer in the HEBS require that the immediate sedimentary environment is highly reducing (cf. Goodfellow and Jonasson 1986); however, the domain of reducing conditions may have been restricted to the sediment porewaters (within the subsurface) or to a chemocline within the water column near the sediment-water interface.

In a redox-stratified ambient paleoenvironment, detrital minerals and/or biogenic debris sinking through the water column and settling on the seafloor may have acquired negative Ce anomalies from the suboxic seawater they travelled through, prior to settling on/in the reducing environment. Such a scenario is shown to have been active at the Moss HEBS locality (Gadd et al., 2019a), where the terrigenous contribution to the HEBS bulk composition is extremely low. At the Monster River locality, the contribution of terrigenous clastic material to the bulk sediment is also low (Fig. 3d), supporting the hypothesis that an overall paucity of clastic sedimentation is a salient control on HEBS formation in Yukon (Gadd and Peter, 2018). The Ce/Ce* values in the siliceous and cherty shale of the Canol Formation sharply increase after HEBS formation (Fig. 3h), suggesting that there was a fundamental shift in physical and/or chemical basinal conditions. The extremely high SiO_2 level (>80 weight %; Fig. 3a) in the basal Canol Formation is consistent with its regional composition (Fraser and Hutchison, 2017; Gadd et al., 2019a; Kabanov, 2019) and signifies a major environmental change. Enhanced SiO_2 deposition is thought to be due to biogenic production from radiolarian blooms fueled by a high degree of paleoproductivity (Fraser and Hutchison, 2017).

The extent to which the clastic sedimentary rocks have been influenced by authigenic or hydrogenous input of REE-Y can be evaluated using Y/Ho ratios. This ratio is tightly coupled in marine environments because Y and Ho are geochemical 'twins', but Ho is much more reactive to scavenging by particulate ferromanganese oxyhydroxides (Bau and Dulski, 1996; Bau, 1999). Scavenging of Ho relative to Y from seawater produces seawater Y/Ho ratios (44–74; Bau, 1996) that are higher than bulk continental crust and clastic sedimentary rocks, both of which have a consistent Y/Ho of 27.7 (McLennan, 2001). Most of the rocks at Monster River have a Y/Ho greater than 27.7 and less than 44, indicating that seawater variably influenced the REE-Y budget of the bulk rock composition.

The Y/Ho ratios of the HEBS samples are higher than the host sedimentary rocks. This suggests that a moderate to significant contribution of these elements (and other REE) was from ambient seawater. Hyper-enriched black shale at the Peel River, Moss, and Nick prospects are characterized by high Y/Ho ratios (Pagès et al., 2018; Crawford et al., 2019; Gadd et al., 2019a), and have geochemically comparable polymetallic HEBS mineralization to the early Cambrian Niutitang Formation in China (Xu et al., 2013; Pagès et al., 2018). The Y/Ho ratios (for all rocks, including HEBS) are strongly negatively correlated with Ce/Ce* anomalies (Fig. 4c). We interpret this to be the result of hydrogenous scavenging by a particulate shuttle that increases the seawater Y/Ho and concomitantly decreases the Ce/Ce* values.

Molybdenum and uranium geochemistry

The bulk Mo abundance in fine-grained marine sedimentary rocks is a robust indicator of the presence and extent of euxinia in ancient depositional environments (Scott and Lyons, 2012), assuming that Mo is hydrogenous and that dilution by clastic (or carbonate) detritus, fluctuations in pH, or low aqueous Mo concentrations did not affect the bulk Mo abundance. Scott and Lyons (2012) define three abundance ranges for Mo in shale that can be used to determine the extent of euxinia: 1) >2 to 25 ppm (indicative of sulfidic porewaters, but not a euxinic water column), 2) 25 to 100 ppm (indicative of an intermittently euxinic to persistent euxinic water column), and 3) >100 ppm (indicative of sustained euxinia). Thermal maturity of organic-rich sediments has been shown to potentially complicate the use of Mo abundance data as a redox proxy (Ardakani et al., 2016). Although organic matter in the shales that host HEBS is beyond the gas window (Peter et al., 2020), this is unlikely to have significantly affected the validity of Mo as a redox proxy because there is a wide range of Mo abundances in the shale samples from the Monster River showing (Fig. 3g; Slack et al., 2017), as well as a positive correlation between Mo and TOC (not shown). Within HEBS mineralization, however, Mo abundance is a less robust redox proxy (Ardakani et al., 2016) because much of the Mo inventory resides within sulfide minerals rather than associated with organic matter (Gadd and Peter, 2018; Gadd et al., 2019b). Similar to the HEBS showings at Moss (Gadd et al., 2019a)

and Peel River (Crawford et al., 2019), the Mo content of the Road River Group rocks at Monster River systematically increases stratigraphically upward to the contact with the HEBS layer (Fig. 3g). This indicates that sulfidic porewaters transitioned to euxinic bottom-waters as a basin-scale phenomenon within the ambient paleoenvironment in which HEBS formed at Monster River.

Molybdenum is trapped in sediments during sulfidic diagenesis, but its delivery to the sediments is enhanced by ferromanganese particulate shuttling (i.e. ferromanganese oxyhydroxide chemical sediments that form in oxygenated seawater; Koschinsky and Hein, 2017). Authigenic Mo (Mo_{EF}) and authigenic U (U_{EF}) relationships are commonly used to assess the role of particulate shuttling and discriminate different depositional environments in shale basins (Fig. 5; Algeo and Tribovillard, 2009). The relationship between Mo_{EF} and U_{EF} may elucidate basinal processes because the marine cycling of these redox-sensitive trace elements responds to sedimentation and basin water restriction (Algeo and Tribovillard, 2009; Tribovillard et al., 2012; Cheng et al., 2016). Both elements are particle-reactive, but only Mo is retained during diagenesis in sulfidic sediments (Algeo and Tribovillard, 2009). Within the sediments molybdates are thiolated (i.e. HS^- replaces O_{2-} in MoO_4^{2-}) and may be sequestered by Fe sulfide minerals and not released back into the water column (Helz et al., 2011). Uranium retention within sulfidic sediments is much less efficient than the retention of molybdenum, and it is released back into the water column (Algeo and Tribovillard, 2009). The low authigenic Mo/U ratios ($Mo_{EF}/U_{EF} \approx 3$) suggest that particulate shuttling was weak; however, this ratio increases markedly within the top 50 cm (Fig. 3j) of the Road River Group and into the HEBS, and remains high in the basal Canol Formation. This suggests that sedimentation of ferromanganese oxyhydroxide particulates intensified and peaked during and after HEBS formation. Intensification of the particulate shuttle may also explain the concomitantly decreasing and increasing values of Ce/Ce* and Y/Ho, respectively (Fig. 4b). In this particulate shuttle scenario, the ferromanganese particles (originally with positive Ce/Ce* and low Y/Ho) dissolved in the sediments, whereas the sinking detritus retained the Ce-depleted and Y-enriched signatures.

Based on these geochemical indicators, it is likely that a particulate shuttle was widespread during the Middle to early Upper Devonian along the Laurentian continental margin. Gadd et al. (2019a) provide strong evidence for particulate shuttling at the Moss showing. Fraser and Hutchison (2017) present authigenic Mo and U data for time-stratigraphically equivalent rocks at Trail River in the eastern Richardson

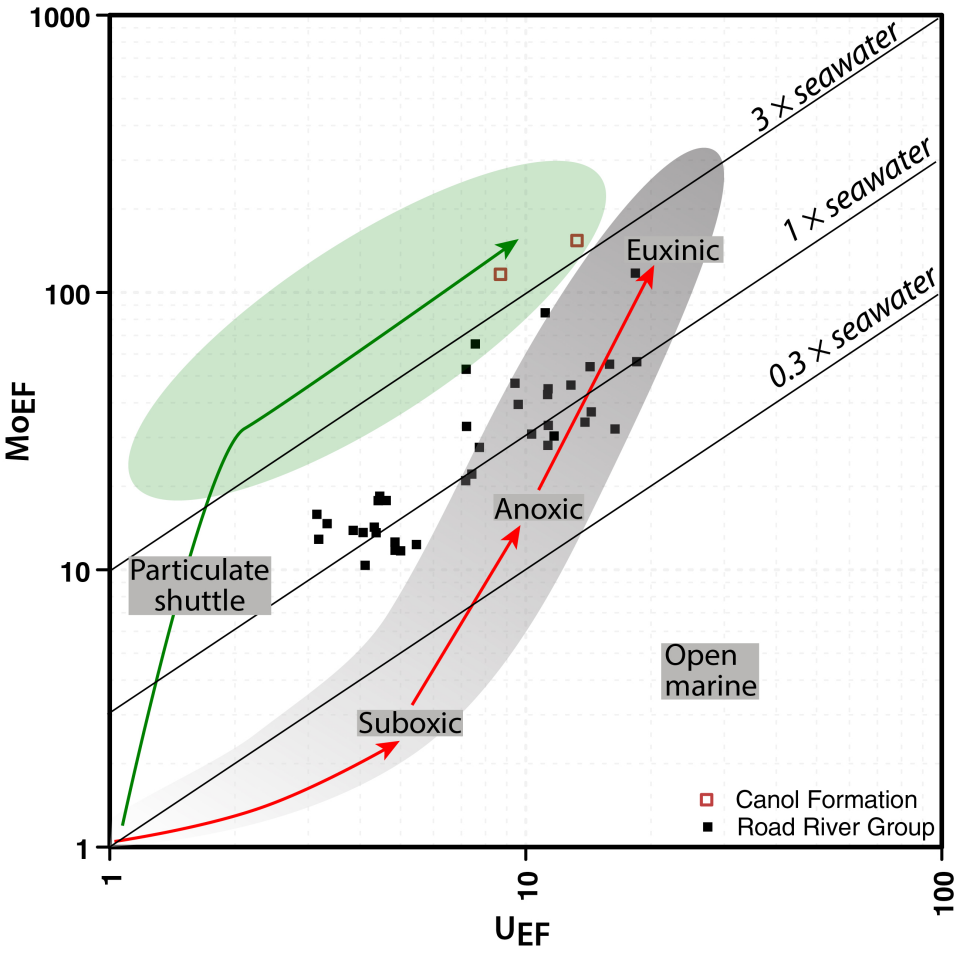

Figure 5. Scatterplot of authigenic Mo (Mo_{EF}) versus authigenic U (U_{EF}) from Canol Formation and Road River Group (RRG) samples of the Monster River showing using fields from Algeo and Tribovillard (2009). The green line (arrow) and green-shaded field represent the trajectory of an active particulate shuttle (*after* Tribovillard et al., 2012). The red line (arrows) and grey-shaded field represent reduction-oxidation zonation in unrestricted (i.e. open) marine environments (*after* Tribovillard et al., 2012).

Mountains that document strong evidence of a particulate shuttle in the water column. The particulate shuttle at Trail River was initiated during the deposition of the Road River Group–Canol Formation transition zone (a weakly mineralized HEBS equivalent) and the Canol Formation. Kabanov (2019) similarly presents authigenic Mo and U data for age-equivalent, correlative rocks on the Mackenzie platform that indicate the presence of an active particulate shuttle. The extensive Mo- and TOC-enriched sediments spanning basinal to platformal sequences is most likely related to major sea level transgressions (Fraser and Hutchison, 2017; Gadd and Peter, 2018; Gadd et al., 2019a), which are well documented throughout the Middle Devonian (Haq and Schutter, 2008).

Metal sources

Metal sources and transport pathways for HEBS are commonly debated because there are no obvious indicators that record the processes responsible for mineralization; moreover, the concentration of metals of potential economic interest is commonly confined to a narrow stratigraphic interval that is geographically widespread (e.g. a regional stratigraphic contact). Hyper-enriched black shales typically contain metals that are common in ultramafic and mafic intrusive complexes, but no such rocks are present in the vicinity or region of HEBS deposits in Yukon. Even though few clues are preserved to offer insight into the origin of HEBS, the regionally consistent characteristics (age, geochemistry, mineralogy) of HEBS deposits that are hundreds of kilometres apart suggests that there is a common origin at the regional scale. Mineralization of HEBS deposits at several localities in Yukon has been interpreted to be the product of highly efficient scavenging of metals from seawater (Gadd and Peter, 2018; Pagès et al., 2018; Gadd et al., 2019a, b). Similarly, HEBS in China are also thought to have formed in this manner (Lehmann et al., 2007, 2016; Xu et al., 2011, 2013; Pagès et al., 2018).

Seawater contains myriad dissolved elements, including those present in HEBS. Although total abundances are low in seawater, biological and chemical sedimentological processes can concentrate and accumulate significant quantities. Nickel, for example, is a bioessential trace element that is incorporated in marine phytoplankton (Piper and Calvert, 2009), methanogenic archaea, and sulfate-assimilating methanotrophs (Konhauser et al., 2009). Assuming high degrees of primary productivity and with highly efficient remineralization of pelagic organic matter, it is possible to accumulate significant (i.e. weight %) abundances of Ni (Lehmann et al., 2016). Nickel is not only concentrated in biomass, but also in chemical sedimentary Fe-Mn particulates (Koschinsky and Hein, 2017). These chemical sediments scavenge hundreds to thousands of parts per million Ni from seawater, where Ni^{2+} is sequestered by weakly negatively charged MnO(OH) (Koschinsky and Hein, 2003). As demonstrated above, there is ample evidence for particulate shuttling (at Monster River, and regionally). We posit that reductive dissolution of Mn particles below the chemocline releases Ni that may in turn be sequestered by the sinking Fe or organic flux (*see* Gadd, Peter, and Layton-Matthews, this volume). We extend this interpretation to the Monster River showing, too, as it possesses all of the hallmark features present in HEBS elsewhere in Yukon (Gadd, Peter, and Layton-Matthews, this volume).

CONCLUSIONS

The presence of HEBS mineralization at Monster River shows that such deposits in northern Yukon extend beyond the confines of the Richardson trough. This indicates that a wide swath of the (?)shelf to slope environment was favourable for the development and preservation of HEBS mineralization and the combination of periodic restriction and ventilation in a continent-marginal setting (trough) is requisite for the formation and preservation of HEBS. Similar to other HEBS localities, the sedimentary environment shifted dramatically across the transition between the Road River Group and Canol Formation at approximately the Eifelian–Givetian stage boundary of the Middle Devonian. Terrigenous detritus predominates within the strata underlying, and up to, the HEBS, after which the terrigenous clastic supply diminished significantly. The hiatus of terrigenous sedimentation marked the onset of condensed sedimentation that is perhaps a fundamental, requisite control on the genesis of HEBS. The HEBS is terminated by the onset of biogenic, silica-dominant sedimentation of the Canol Formation.

Lithogeochemical data for the host rocks and HEBS show that the paleoenvironmental redox conditions likely fluctuated between suboxic, anoxic, and euxinic. The REE-Y systematics of the immediate host rocks and HEBS suggest a predominantly suboxic marine environment, whereas the Mo abundances provide evidence that suggests transiently anoxic to euxinic conditions. The contradictory redox proxies are interpreted to reflect redox stratification where the chemocline is situated near the sediment-water interface. Authigenic enrichments of Mo and U, uniformly negative Ce anomalies, and superchondritic Y/Ho ratios collectively indicate that particulate shuttling transferred metals to the seafloor, and that the HEBS was deposited at the peak of hydrogenous ferromanganese particulate sedimentation. These data signify a basinal environment that experienced varying degrees of restriction and stratification, during which pulses of fresh (i.e. unfractionated) marine waters delivered metals, metalloids, and sulfur. This type of geological setting is considered critical to the formation and preservation of HEBS mineralization.

ACKNOWLEDGMENTS

Support for this study was provided through Targeted Geoscience Initiative 5 Volcanic- and Sedimentary-Hosted Base Metal Ore System Activity VS-1.2: Development of genetic and exploration models for hyper-enriched black shale (HEBS) deposits. Additional funding and field logistical support came from the Polar Continental Shelf program (project 010-18). We thank Daniel Gregory and Pavel Kabanov for their reviews. We also thank Krebchov Haimbodi of Queen's University for his assistance in the field. This is Yukon Geological Survey Contribution 045.

REFERENCES

Algeo, T.J. and Tribovillard, N., 2009. Environmental analysis of paleoceanographic systems based on molybdenum–uranium covariation; Chemical Geology, v. 268, no. 3-4, p. 211–225. https://doi.org/10.1016/j.chemgeo.2009.09.001

Alibo, D.S. and Nozaki, Y., 1999. Rare earth elements in seawater: particle association, shale-normalization, and Ce oxidation; Geochimica et Cosmochimica Acta, v. 63, no. 3-4, p. 363–372. https://doi.org/10.1016/S0016-7037(98)00279-8

Ardakani, O.H., Chappaz, A., Sanei, H., and Mayer, B., 2016. Effect of thermal maturity on remobilization of molybdenum in black shales; Earth and Planetary Science Letters, v. 449, p. 311–320. https://doi.org/10.1016/j.epsl.2016.06.004

Bau, M., 1996. Controls on the fractionation of isovalent trace elements in magmatic and aqueous systems: evidence from Y/Ho, Zr/Hf, and lanthanide tetrad effect; Contributions to Mineralogy and Petrology, v. 123, no. 3, p. 323–333. https://doi.org/10.1007/s004100050159

Bau, M. and Dulski, P., 1996. Distribution of yttrium and rare-earth elements in the Penge and Kuruman iron-formations, Transvaal Supergroup, South Africa; Precambrian Research, v. 79, no. 1-2, p. 37–55. https://doi.org/10.1016/0301-9268(95)00087-9

Carne, R.C., 1989. Report on Nick property; Yukon Geological Survey, Yukon Geological Survey, Energy, Mines and Resources Property File Collection, ARMC005013, 8 p. <http://ygsftp.gov.yk.ca/publications/anvil_records/faro_files/005000-005999/005013.pdf>

Cecile, M.P., Morrow, D.W., and Williams, G.K., 1997. Early Paleozoic (Cambrian to Early Devonian) tectonic framework, Canadian Cordillera; Bulletin of Canadian Petroleum Geology, v. 45, no. 1, p. 54–74. https://doi.org/10.35767/gscpgbull.45.1.054

Cheng, M., Li, C., Zhou, L., Algeo, T.J., Zhang, F., Romaniello, S., Jin, C., Lei, L., Feng, L., and Jiang, S.Y., 2016. Marine Mo biogeochemistry in the context of dynamically euxinic mid-depth waters: a case study of the lower Cambrian Niutitang shales, South China; Geochimica et Cosmochimica Acta, v. 183, p. 79–93. https://doi.org/10.1016/j.gca.2016.03.035

Crawford, I., Layton-Matthews, D., Peter, J.M., Gadd, M.G., and Voinot, A., 2019. Toward the application of molybdenum and thallium isotopes as indicators of paleoredox conditions and genesis of hyper-enriched black shale (HEBS) deposits, Peel River, Yukon, *in* Targeted Geoscience Initiative: 2018 report of activities, (ed.) N. Rogers; Geological Survey of Canada, Open File 8549, p. 139–161.

De Baar, H.J.W., German, C.R., Elderfield, H., and van Gaans, P., 1988. Rare-earth element distributions in anoxic waters of the Cariaco Trench; Geochimica et Cosmochimica Acta, v. 52, no. 5, p. 1203–1219. https://doi.org/10.1016/0016-7037(88)90275-X

Dumala, M., 2007. Assessment report describing prospecting and geological mapping at the Mon property; prepared for Southampton Ventures Inc. and Strategic Metals Ltd.: Whitehorse, Yukon Territory, 37 p. <http://yma.gov.yk.ca/094890.pdf> [accessed January 8, 2020]

Elderfield, H. and Greaves, M.J., 1982. The rare earth elements in seawater; Nature, v. 296, p. 214–218. https://doi.org/10.1038/296214a0

Fraser, T.A. and Hutchison, M.P., 2017. Lithogeochemical characterization of the Middle–Upper Devonian Road River Group and Canol and Imperial formations on Trail River, east Richardson Mountains, Yukon: age constraints and a depositional model for fine-grained strata in the Lower Paleozoic Richardson trough; Canadian Journal of Earth Sciences, v. 54, no. 7, p. 731–765. https://doi.org/10.1139/cjes-2016-0216

Gadd, M.G. and Peter, J.M., 2018. Field observations, mineralogy and geochemistry of Middle Devonian Ni-Zn-Mo-PGE hyper-enriched black shale deposits, Yukon; *in* Targeted Geoscience Initiative: 2017 report of activities, volume 1, (ed.) N. Rogers; Geological Survey of Canada, Open File 8358, p. 193–206. http://doi.org/10.4095/306475

Gadd, M.G., Layton-Matthews, D., and Peter, J.M., 2016, Non-hydrothermal origin of apatite in SEDEX mineralization and host rocks of the Howard's Pass district, Yukon, Canada: American Mineralogist, v. 101, p. 1061-1071.

Gadd, M.G., Peter, J.M., Goodfellow, W., Jackson, S.E., and Yang, Z., 2017. Geology, geochemistry and mineralogy of hyper-enriched black shale deposits, Yukon; *in* Proceedings of Exploration 17: Sixth Decennial International Conference on Mineral Exploration, Toronto, Canada, 2017, (ed.) V. Tschirhart and M.D. Thomas; Decennial Mineral Exploration Conferences, p. 841–845.

Gadd, M.G., Peter, J.M., Fraser, T.A., and Layton-Matthews, D., 2019a. Lithogeochemical and sulphur isotope indicators of environment of formation and genesis of the Moss hyper-enriched black shale showing, Yukon; *in* Targeted Geoscience Initiative: 2018 report of activities, (ed.) N. Rogers; Geological Survey of Canada, Open File 8549, p. 163–178. https://doi.org/10.4095/313648

Gadd, M.G., Peter, J.M., Jackson, S.E., Yang, Z., and Petts, D., 2019b. Platinum, Pd, Mo, Au and Re deportment in hyper-enriched black shale Ni-Zn-Mo-PGE mineralization, Peel River, Yukon, Canada; Ore Geology Reviews, v. 107, p. 600–614. https://doi.org/10.1016/j.oregeorev.2019.02.030

Gadd, M.G., Peter, J.M., Hnatyshin, D., Creaser, R., Gouwy, S.A., and Fraser, T.A., 2020. A Middle Devonian basin-scale precious metal enrichment event across northern Yukon (Canada): Geology, v. 48, no. 3, p. 242–246. https://doi.org/10.1130/G46874.1

German, C.R. and Elderfield, H., 1990. Application of the Ce anomaly as a paleoredox indicator: the ground rules; Paleoceanography and Paleoclimatology, v. 5, no. 5, p. 823–833. https://doi.org/10.1029/PA005i005p00823

Gordey, S.P. and Anderson, R.G., 1993. Evolution of the northern Cordilleran miogeocline, Nahanni map area (105I), Yukon and Northwest Territories; Geological Survey of Canada, Memoir 428, 214 p https://doi.org/10.4095/183983

Haq, B. and Schutter, S., 2008, A chronology of Paleozoic sea-level changes; Science, v. 322, p. 64–68. https://doi.org/10.1126/science.1161648

Helz, G.R., Bura-Nakić, E., Mikac, N., and Ciglenečki, I., 2011. New model for molybdenum behavior in euxinic waters; Chemical Geology, v. 284, no. 3-4, p. 323–332. https://doi.org/10.1016/j.chemgeo.2011.03.012

Himmler, T., Bach, W., Borhmann, G., and Peckmann, J., 2010. Rare earth elements in authigenic methane-seep carbonates as tracers for fluid composition during early diagenesis; Chemical Geology, v. 277, no. 1-2, p. 126–136. https://doi.org/10.1016/j.chemgeo.2010.07.015

Horan, M.F., Morgan, J.W., Grauch, R.I., Coveney, R.M., Jr., Murowchick, J.B., and Hulbert, L.J., 1994. Rhenium and osmium isotopes in black shales and Ni-Mo-PGE-rich sulfide layers, Yukon Territory, Canada, and Hunan and Guizhou provinces, China; Geochimica et Cosmochimica Acta, v. 58, no. 1, p. 257–265. https://doi.org/10.1016/0016-7037(94)90463-4

Hu, Y., Feng, D., Peckmann, J., Roberts, H.H., and Chen, D., 2014. New insights into cerium anomalies and mechanisms of trace metal enrichment in authigenic carbonate from hydrocarbon seeps; Chemical Geology, v. 381, p. 55–66. https://doi.org/10.1016/j.chemgeo.2014.05.014

Hulbert, L.J., Gregoire, D.C., Paktunc, D., and Carne, R.C., 1992. Sedimentary nickel, zinc, and platinum-group-element mineralization in Devonian black shales at the Nick property, Yukon, Canada: a new deposit type; Exploration and Mining Geology, v. 1, no. 1, p. 39–62.

Jambor, J.L., Nordstrom, D.K., and Alpers, C. N., 2000. Metal-sulfate salts from sulfide mineral oxidation; Reviews in Mineralogy and Geochemistry, v. 40, p. 303–350.

Kabanov, P., 2019. Devonian (c. 388–375 Ma) Horn River Group of Mackenzie platform (NW Canada) is an open-shelf succession recording oceanic anoxic events; Journal of the Geological Society, v. 176, p. 29–45. https://doi.org/10.1144/jgs2018-075

Koschinsky, A., and Hein, J. R., 2003, Uptake of elements from seawater by ferromanganese crusts: solid-phase associations and seawater speciation; Marine Geology, v. 198, no. 3-4, p. 331–351. https://doi.org/10.1016/S0025-3227(03)00122-1

Koschinsky, A. and Hein, J.R., 2017. Marine ferromanganese encrustations: archives of changing oceans; Elements, v. 13, no. 3, p. 177–182. https://doi.org/10.2113/gselements.13.3.177

Konhauser, K.O., Pecoit, E., Lalonde, S., Papineau, D., Nisbet, E., Barley, M.E., Arndt, N., Zahnle, K., and Kamber, B.S., 2009. Oceanic nickel depletion and a methanogen famine before the Great Oxidation Event; Nature, v. 458, no. 7239, p. 750–753. https://doi.org/10.1038/nature07858

Lehmann, B., Nägler, T.F., Holland, H.D., Wille, M., Mao, J., Pan, J., Ma, D., and Dulski, P., 2007. Highly metalliferous carbonaceous shale and Early Cambrian seawater; Geology, v. 35, no. 5, p. 403–406. https://doi.org/10.1130/G23543A.1

Lehmann, B., Frei, R., Xu, L., and Mao, J., 2016. Early Cambrian black shale-hosted Mo-Ni and V mineralization on the rifted margin of the Yangtze platform, China: reconnaissance chromium isotope data and a refined metallogenic model; Economic Geology, v. 111, no. 1, p. 89–103. https://doi.org/10.2113/econgeo.111.1.89

Lenz, A.C., 1972. Ordovician to Devonian history of northern Yukon and adjacent District of Mackenzie; Bulletin of Canadian Petroleum Geology, v. 20, no. 2, p. 321–361. https://doi.org/10.35767/gscpgbull.20.2.321

Lode, S., Piercey, S.J., and Devine, C.M., 2015. Geology, mineralogy, and lithogeochemistry of metalliferous mudstones associated with the Lemarchant volcanogenic massive sulfide deposit, Tally Pond belt, central Newfoundland; Economic Geology, v. 110, no. 7, p. 1835–1859. https://doi.org/10.2113/econgeo.110.7.1835

McLennan, S.M., 1989. Rare-earth elements in sedimentary-rocks: influence of provenance and sedimentary processes; Reviews in Mineralogy and Geochemistry, v. 21, p. 169–200.

McLennan, S.M., 2001. Relationships between the trace element composition of sedimentary rocks and upper continental crust; Geochemistry, Geophysics, Geosystems, v. 2, no. 4, p. 1–24. https://doi.org/10.1029/2000GC000109

Morrow, D., 1999. Lower Paleozoic stratigraphy of northern Yukon Territory and northwestern District of Mackenzie; Geological Survey of Canada, Bulletin 538, 202 p. https://doi.org/10.4095/210998

Morrow, D.W. and Geldsetzer, H.J., 1988. Devonian of the eastern Canadian Cordillera; *in* Devonian of the world, volume 1: regional syntheses, (ed.) N.J. McMillan, A.F. Embry, and D.J. Glass; Canadian Society of Petroleum Geologists, Memoir 14, p. 85–121.

Norris, A.W., 1985. Stratigraphy of Devonian outcrop belts in northern Yukon Territory and northwestern District of Mackenzie (Operation Porcupine area); Geological Survey of Canada, Memoir 410, 81 p. https://doi.org/10.4095/120309

Norris, A.W. 1997. Devonian; Chapter 7 *in* Geology and mineral and hydrocarbon potential of northern Yukon Territory and northwestern District of Mackenzie, (ed.) D.K. Norris; Geological Survey of Canada, Bulletin 422, p. 163–200. https://doi.org/10.4095/208893

Nozaki, Y., 1997. A fresh look at element distribution in the north Pacific Ocean; Eos, Transactions of the American Geophysical Union, v. 78, no. 21, p. 221–223. https://doi.org/10.1029/97EO00148

Orberger, B., Pasava, J., Gallien, J.P., and Daudin, L., 2003a. Se, As, Mo, Ag, Cd, In, Sb, Pt, Au, Tl, Re traces in biogenic and abiogenic sulfides from black shales (Selwyn Basin, Yukon territories, Canada): a nuclear microprobe study; Nuclear Instruments and Methods in Physics Research Section B: Beam Interactions with Materials and Atoms, v. 210, p. 441–448. https://doi.org/10.1016/S0168-583X(03)01073-5

Orberger, B., Pasava, J., Gallien, J.P., Daudin, L., and Pinti, D.L., 2003b. Biogenic and abiogenic hydrothermal sulfides: controls of rare metal distribution in black shales (Yukon Territories, Canada); Journal of Geochemical Exploration, v. 78–79, p. 559–563. https://doi.org/10.1016/S0375-6742(03)00141-9

Orberger, B., Gallien, J.P., Pinti, D.L., Fialin, M., Daudin, L., Gröcke, D.R., and Pasava, J., 2005. Nitrogen and carbon partitioning in diagenetic and hydrothermal minerals from Paleozoic black shales, (Selwyn Basin, Yukon Territories, Canada); Chemical Geology, v. 218, no. 3-4, p. 249–264. https://doi.org/10.1016/j.chemgeo.2005.01.012

Pagès, A., Barnes, S., Schmid, S., Coveney, R.M., Jr., Schwark, L., Liu, W., Grice, K., Fan, H., and Wen, H., 2018. Geochemical investigation of the lower Cambrian mineralised black shales of South China and the late Devonian Nick deposit, Canada; Ore Geology Reviews, v. 94, p. 396–413. https://doi.org/10.1016/j.oregeorev.2018.02.004

Pasava, J., Chrastny, V., Loukola-Ruskeeniemi, K., and Sebek, O., 2018. Nickel isotopic variation in black shales from Bohemia, China, Canada, and Finland: a reconnaissance study; Mineralium Deposita, v. 54, no. 5, p. 719–742. https://doi.org/10.1007/s00126-018-0839-8

Peter, J.M., Goodfellow, W.D., and Doherty, W., 2003, Hydrothermal sedimentary rocks of the Heath Steele belt, Bathurst mining camp, New Brunswick: Part 2. Bulk and rare earth element geochemistry and implications for origin; *in* Massive sulfide deposits of the Bathurst Mining Camp, New Brunswick, and northern Maine, (ed.) W.D. Goodfellow, S.R. McCutcheon, and J.M. Peter; Economic Geology Monograph 11, p. 391–415. https://doi.org/10.5382/Mono.11.17

Piper, D.Z. and Calvert, S.E., 2009. A marine biogeochemical perspective on black shale deposition; Earth-Science Reviews, v. 95, no. 1-2, p. 63–96. https://doi.org/10.1016/j.earscirev.2009.03.001

Reynard, B., Lecuyer, C., and Grandjean, P., 1999. Crystal-chemical controls on rare-earth element concentrations in fossil biogenic apatites and implications for paleoenvironmental reconstructions; Chemical Geology, v. 155, no. 3-4, p. 233–241. https://doi.org/10.1016/S0009-2541(98)00169-7

Scott, C. and Lyons, T., 2012. Contrasting molybdenum cycling and isotopic properties in euxinic versus non-euxinic sediments and sedimentary rocks: refining the paleoproxies; Chemical Geology, v. 324-325, p. 19–27. https://doi.org/10.1016/j.chemgeo.2012.05.012

Slack, J.F., Grenne, T., and Bekker, A., 2009. Seafloor-hydrothermal Si-Fe-Mn exhalites in the Pecos greenstone belt, New Mexico, and the redox state of ca. 1720 Ma deep seawater; Geosphere, v. 5, no. 3, p. 302–314. https://doi.org/10.1130/GES00220.1

Slack, J.F., Falck, H., Kelley, K., and Xue, G., 2017. Geochemistry of host rocks in the Howards Pass district, Yukon-Northwest Territories, Canada: implications for sedimentary environments of Zn-Pb and phosphate mineralization; Mineralium Deposita, v. 52, no. 4, p. 565–593. https://doi.org/10.1007/s00126-016-0680-x

Steiner, M., Wallis, E., Erdtmann, B.-D., Zhao, Y., and Yang, R., 2001. Submarine-hydrothermal exhalative ore layers in black shales from South China and associated fossils—insights into a Lower Cambrian facies and bio-evolution; Palaeogeography, Palaeoclimatology, Palaeoecology, v. 169, no. 3-4, p. 165–191. https://doi.org/10.1016/S0031-0182(01)00208-5

Tribovillard, N., Algeo, T.J., Lyons, T., and Riboulleau, A., 2006. Trace metals as paleoredox and paleoproductivity proxies: an update; Chemical Geology, v. 232, no. 1-2, p. 12–32. https://doi.org/10.1016/j.chemgeo.2006.02.012

Tribovillard, N., Algeo, T.J., Baudin, F., and Riboulleau, A., 2012. Analysis of marine environmental conditions based onmolybdenum–uranium covariation—applications to Mesozoic paleoceanography; Chemical Geology, v. 324-325, p. 46–58. https://doi.org/10.1016/j.chemgeo.2011.09.009

Wallace, M.W., Hood, A.vS., Shuster, A.M., Greig, A., Planavsky, N.J., and Reed, C.P., 2017. Oxygenation history of the Neoproterozoic to early Phanerozoic and the rise of land plants; Earth and Planetary Science Letters, v. 466, p. 12–19. https://doi.org/10.1016/j.epsl.2017.02.046

Wright, J., Schrader, H., and Holser, W.T., 1987. Paleoredox variations in ancient oceans recorded by rare earth elements in fossil apatite; Geochimica et Cosmochimica Acta, v. 51, no. 3, p. 631–644. https://doi.org/10.1016/0016-7037(87)90075-5

Xu, L., Lehmann, B., Jingwen, M., Wenjun, Q., and Andao, D., 2011. Re-Os age of polymetallic Ni-Mo-PGE-Au mineralization in Early Cambrian black shales of south China—a reassessment; Economic Geology, v. 106, no. 3, p. 511–522. https://doi.org/10.2113/econgeo.106.3.511

Xu, L., Lehmann, B., and Mao, J., 2013. Seawater contribution to polymetallic Ni–Mo–PGE–Au mineralization in Early Cambrian black shales of South China: evidence from Mo isotope, PGE, trace element, and REE geochemistry; Ore Geology Reviews, v. 52, p. 66–84. https://doi.org/10.1016/j.oregeorev.2012.06.003